



An eco-friendly method for preventing corrosion in low-carbon steel using an extract from *Guazma tomentosa* leaves.

¹Rajabhuvaneswari Ariyamuthu,

Professor, Department of Chemistry, Bharath Institute of Higher Education and Research, Selaiyur, Tambaram, Chennai – 600 073.

²Lavanya S,

Assistant Professor, Department of Chemistry, Velammal College of Engineering and Technology, Madurai

³Jeevalatha Rugmangathan,

Assistant Professor, Department of Chemistry, Panimalar Engineering College, Chennai-600029, Tamilnadu, India

(Received: 07 October 2023

Revised: 12 November

Accepted: 06 December)

KEYWORDS

Corrosion metal, Inhibition efficiency, Potentiodynamic polarization, Electrochemical impedance, Tafel plot.

Abstract

Corrosion engineers now consider low-carbon steel an absolute must for industrial applications. According to organic compounds, N, S, O, and heterocyclic chemicals with polar functional groups and conjugated double bonds in the extract showed promise as inhibitors. Powder X-ray diffraction and energy-dispersive X-ray spectroscopy investigations supplemented the scanning electron microscopy (SEM) to characterize the surface morphologies. An acidic solution was used to conduct corrosion inhibition tests on low-carbon steel with *Guazma tomentosa* (GUTLE) leaf extract. Electrochemical techniques, weight loss, FT-IR, XRD, EDAX, and SEM were employed in these investigations. Thermodynamic investigations are computed and reviewed as well. Thenbachai tree, or *Guazma tomentosa*, is a member of the Sterculiaceae family.

1. Introduction

Acid pickling, industrial cleaning, acid descaling, oil-well acidizing, petrochemical operations, and many more uses for acid solutions make low-carbon steel indispensable with carbon content. Numerous methods have been implemented recently to reduce iron corrosion caused by acids. Applying inhibitors is one method that has been used to lessen corrosion. Enzymes that prevent corrosion include heterocyclic compounds with polar groups, conjugated double bonds, and organic compounds with nitrogen, sulfur, and oxygen [2–5]. These chemicals adsorb to metal surfaces and block corrosion at their active locations [6]. Many chemical molecules are bad for the environment. To address these issues, it is crucial to find corrosion inhibitors made of natural ingredients that are affordable, nontoxic, and environmentally benign.

The organic chemicals are derived from natural spices and medicinal plant leaves. Many organic chemicals are found in plant extracts and can be obtained inexpensively and environmentally friendly. Evidence in the literature shows that compounds can reduce the corrosion of many metals [7–15]. One plant that is widely

available in India is *Guazma tomentosa*. Commonly referred to as the Thenbachai tree, it is a member of the Sterculiaceae family. The compounds found in *Guazma tomentosa* include kaempferol, caffeine, catechins, procyanidins B-2, B-5, and C-1, tartaric acid, xanthan gum, and many more [16]. The intention is to employ the *Guazma tomentosa* leaves (Gutle) extract as a green inhibitor on low-carbon steel in an acidic medium because the plant contains heterocyclic chemicals, and leaves have not yet been utilized. This investigation used various methodologies, including gravimetric studies, electrochemical measurements, and FT-IR, SEM, and EDAX.

2. Experimental

2.1 Preparation of the specimens

Dimensionally, 2.5 X 2.5 X 0.4 cm low carbon steel specimens (C:4.44%, Fe:92.9%, Cr:0.75%) were utilized for the present investigation. The low-carbon steel samples were smoothed out using a 4/0 grit emery paper. After being meticulously rinsed with 100% ethanol, the specimens were allowed to air dry before being carefully placed in a desiccator to ensure they



would not absorb any moisture. At least annular-grade chemicals or reagents were utilized in any way. In this experiment, 1M HCl served as the electrolyte.

2.2 Preparation of GUTLE

The Virudhu Nagar district in the Indian state of Tamil Nadu is where the Guazma tomentosa leaves were gathered. After a seven-day shade drying, the leaves were ground into a fine powder. Ten grams of this powdered leaf material were extracted with 100% ethanol using the Soxhlet apparatus for five hours. Following extraction, the liquid was strained and subjected to a water bath maintained at 55°C until the remaining residue was collected. The stock residue was used to generate six inhibitor sample solutions ranging in concentration from 0 to 250 mg/100 ml of HCl.

2.3 Gravimetric experiments

In each set of samples, which were kept at varying temperatures of 303, 308, 313, 318, 323, and 333K for two hours, the polished and pre-weighed low carbon steel specimens were submerged in 100 cc of the sample as mentioned earlier, and blank solutions. Following the allotted immersion time, the specimens were extracted, washed with water and 100% ethanol, and placed in desiccators for future use. The weight loss was calculated by reweighing the dried specimens. The studies were conducted multiple times to get the most out of each pair of specimens. Equations (1) and (2) were used to compute the corrosion rate (ϵ) and the percentage of inhibition efficiency (IE%) [17]. $\lambda_{(mpy)} =$

$$534 \times \frac{\Delta W}{DAT} \quad (1)$$

$$CapIE\% = \frac{(W_b - W_a)}{W_o} \times 100 \quad (2)$$

In this case ΔW is equal to $(W_b - W_a)$, where W_b and W_a are the specimen weights before and after immersion in the solution. The density of low carbon steel is D grams per cubic centimeter, the area of the specimen is A square inches, and the period of immersion is T hours.

2.4 Electrochemical Assays

An electrochemical workstation impedance analyzer model CHI760D was used to record the Nyquist and Tafel polarization curves. The cell comprises an active platinum electrode, a saturated calomel electrode, and a working electrode. The working electrode was a

low-carbon steel specimen with an exposed area of 0.5 cm². The reference and counter electrodes were made of saturated calomel and platinum, respectively. Various sample solutions were used to immerse the working electrode. Under stationary conditions, 100 cc of electrolyte (1M HCl) was used for all electrochemical tests conducted at 303K. We evaluated the open circuit potential (OCP) of the rusted electrode before performing each potentiodynamic polarization (Tafel) and electrochemical impedance spectroscopy (EIS) test. A scan rate of 0.01 vs-1 was used to record potentiodynamic polarization curves from -250 to +250 mV/SCE (against OCP). At different frequencies, the ohm values for the real and imaginary components of the cell impedance were recorded. Equations (3) and (4) were used to get the values of the double-layer capacitance (C_{dl}) and the charge-transfer resistance (R_{ct}) [18].

$$R_{ct} = (R_s + R_{ct}) - R_s \quad (3)$$

$$C_{dl} = \frac{1}{2} \cdot \pi R_{ct} f_{max} \quad (4)$$

2.5 Fourier Transform Infra-Red spectroscopy (FT-IR)

A Bruker spectrophotometer was used to record the FT-IR spectra. For 2 hours, the FT-IR characterization specimen was submerged in 100 ml of 1M HCl solution containing 250 mg of inhibitor per 100 ml of HCl. The specimen was removed after two hours, allowed to dry, and then prepared into a disk by rubbing it with a small quantity of KBr powder. The Gutle residue underwent the same process as described above, with the addition of recording FT-IR spectra.

2.6 SEM Analysis and EDAX Characterization

The low-carbon steel specimen was submerged in a 1.0 M HCl solution devoid of the ideal inhibitor concentration for two hours. Bruker Scanning Electron Microscopy and EDAX Spectrometer were used for SEM and EDAX characterization after the specimen was dried after the appropriate immersion period.

3. Results and Discussion

3.1 Gravimetric Experiment

The corrosion rate of low carbon steel in 1M HCl in the absence and presence of varying concentrations of. The results of the 303-333K determination of the Guazma tomentosa leaf extracts are



presented in Table 1; for both the control and different concentrations of gentle extract, Figures 1 and 2 show how the corrosion rate and inhibition efficiency changed as a function of concentration. Figure 1 shows that as the inhibitor concentration increases, the corrosion rate of low-carbon steel reduces; this proves that guttle inhibits corrosion of low-carbon steel and that the efficacy of the inhibition is concentration-dependent. Graph 2 shows that as the concentration of the inhibitor rises, the inhibition efficiency of low-carbon steel also rises. At the optimal inhibitor dose of 250 mg/100 ml of HCl, the inhibition efficacy was 87.7 percent, suggesting that Gutle was the most effective inhibitor in the acidic medium. Because low-carbon steel desorbs Gutle from its surface at higher temperatures, the inhibitor efficiency drops as the temperature rises (see Figure 3, which plots inhibition efficiency against temperature for specimens with varying amounts of Gutle) [19,20]. Low carbon steel's corrosion rate drops as the contact time between blank and inhibitor acid solutions increases (Figure 4, a plot of corrosion rate against time for specimens with varying guttle concentrations). Combining iron and inhibitor molecules may reduce accessible inhibitor molecules in the solution, reducing the inhibition efficacy caused by the long immersion period [21].

3.2 Assessments of potentiodynamic polarization

Polarization studies can verify that a protective coating has formed on metal surfaces when inhibiting corrosion. Figure 5 shows the polarization curves for low-carbon steel in a 1MHCl solution, both for the blank and for different inhibitor concentrations. The following electrochemical kinetic parameters are presented in Table 2: corrosion potential (E_{corr}), cathodic and anodic slope (b_c and b_a), corrosion current density (i_{corr}), and percentage of inhibition efficiency (E_{in}). These values were obtained from Tafel curves [22]. The fact that the Gutle functions as a mixed-type inhibitor is supported by the fact that the most significant shift of E_{corr} values in this investigation is 34 mV [18]. Equation (5) [18] was used to calculate the inhibition efficiency (IE%).

$$IE\% = \left(\frac{i_{corr}^o - i_{corr}}{i_{corr}^o} \right) \times 100 \quad (5)$$

Table 2 demonstrates that within the presence of Gutle, corrosion current density (i_{corr}) reduces more than in the blank solution (i.e., i_{corr}^o) owing to an increased blocked percentage of the electrode surface caused by adsorption. The numbers above represent the stages of metal surface protective layer creation. At all concentrations, the anodic reaction was more tightly regulated than the cathodic one, as b_a is less than b_c [17].

The effect of temperature on the inhibitory efficacy of gutle on corrosion of low carbon steel in 1M HCl, as shown in Table 1.

Gutle Residue (mg)	303K		308K		313K		318K		323K		333K	
	CR (mp)	IE (%)	CR (mp)	IE (%)	CR (mp)	IE (%)	CR (mpy)	IE (%)	CR (mpy)	IE (%)	CR (mpy)	IE (%)
0	0.8315	-	0.6181	-	0.4301	-	0.3599	-	0.2612	-	0.2071	-
50	0.4461	46.36	0.3632	41.23	0.2644	38.51	0.223	38.05	0.1975	24.39	0.172	16.92
100	0.3695	55.55	0.2931	52.51	0.2198	48.88	0.2039	43.36	0.1688	35.36	0.1529	26.15
150	0.2739	67.04	0.2262	63.4	0.1879	60	0.1657	53.98	0.1719	52.43	0.1529	46.15
200	0.1943	76.62	0.1784	71.13	0.1434	66.66	0.1211	66.37	0.0987	62.19	0.0892	56.92
250	0.1019	87.73	0.1083	82.47	0.1019	76.29	0.0924	74.33	0.0669	74.39	0.0669	67.69

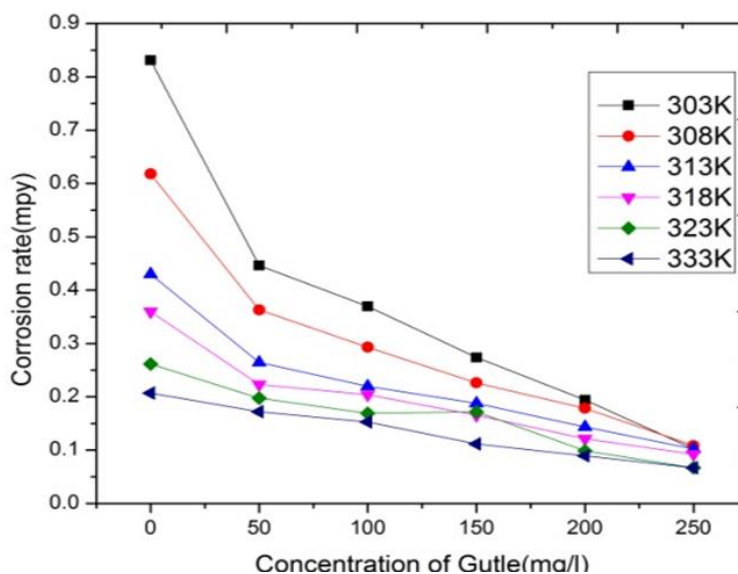


Figure .1 Corrosion rate of low carbon steel in 1MHCl with and without inhibitor

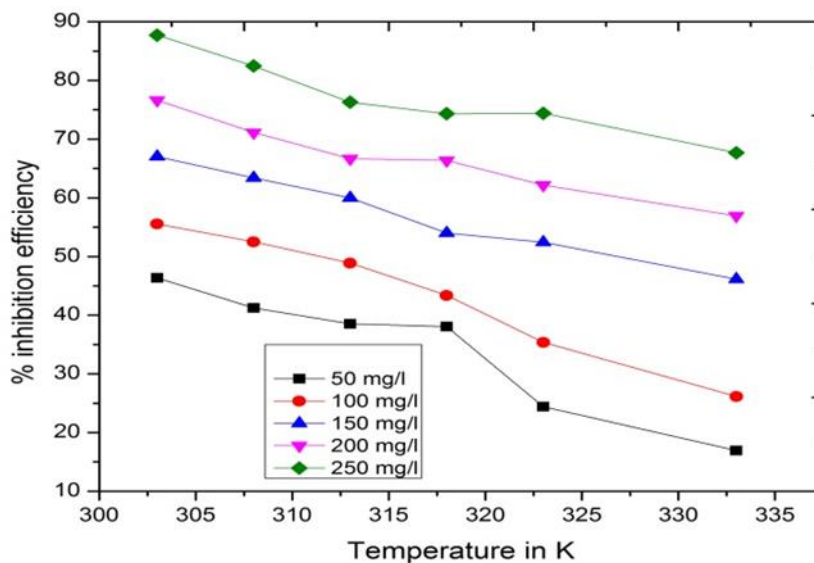


Figure .2 Variation of inhibition efficiency of low carbon steel with and without inhibitor in 1MHCl at different temperatures

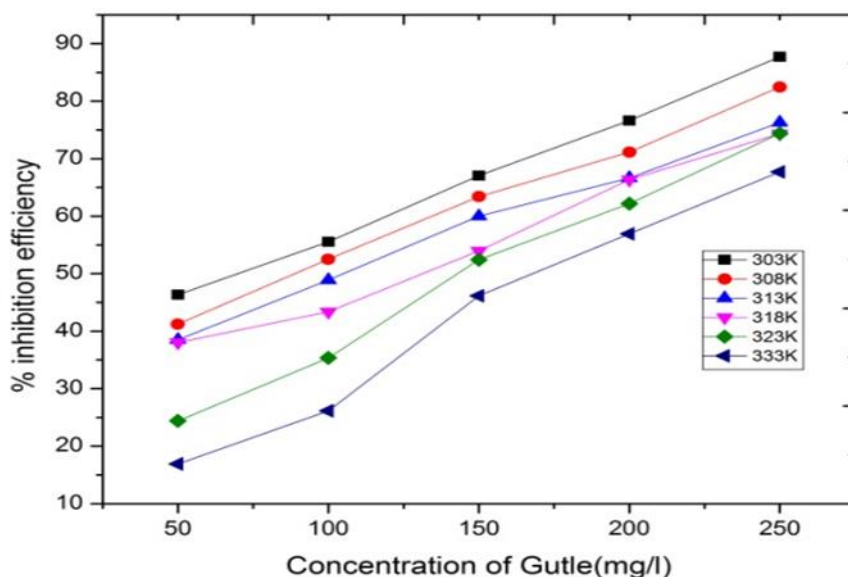


Figure .3 Inhibition Efficiency with temperature in the presence of different concentrations of *Gutle*

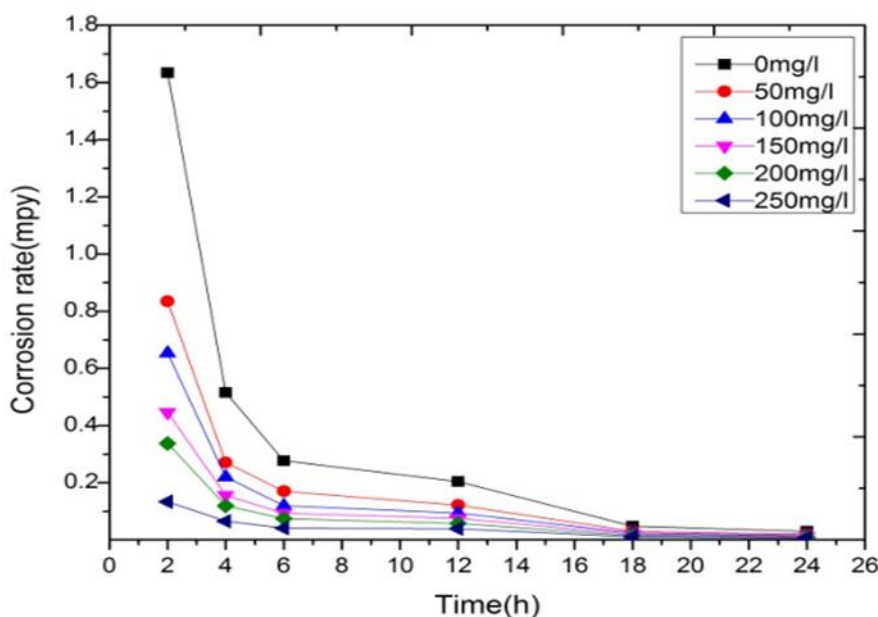


Figure .4 Corrosion rate of *Gutle* as a function of time in 1M HCl

3.3 Electrochemical impedance measurements

Figure 6 shows Nyquist plots of low-carbon steel in 1M HCl with and without different doses of guile inhibitors. The impedance characteristics obtained from Nyquist plots, including R_s , R_{ct} , C_{dl} , and f_{max} , are listed in Table 2. Following this equation (6) [17], we calculated the inhibition efficiency percentage.

$$IE\% = \left(\frac{R_{ct(inh)} - R_{ct}}{R_{ct(inh)}} \right) \times 100 \quad (6)$$

As the concentration of *Gutle* in an acid solution grows, the charge-transfer resistance also increases, which means the protective adsorption layer has formed. The creation of a protective layer on the metal surface is confirmed by the increasing charge transfer resistance value (R_{ct}) and percentage of inhibitory efficiency (%IE)



when the concentration of Gutle increases, as shown in Table.2 [23,24]. A lower value for the double layer capacitance (Cdl) is observed when the concentration of the gutle increases. A decline in double-layer capacitance (Cdl) and an increase in inhibition efficiency (%IE) are both seen in Table 3. The adsorption of inhibitor molecules on the metal surface is indicated by the

Nyquist plot's diameter increasing with the concentration of the Gutle. The establishment of a protective layer on the surface of low-carbon steel is confirmed by the increase in the diameter of the Nyquist plot, the value of the charge transfer resistance (Rct), and the double-layer capacitance (Cdl) [25].

Table .2 Potentiodynamic polarization parameters for low-carbon steel corrosion in 1MHCl with varying concentrations of gutle

<i>Gutle residue</i> (mg)	E_{corr} (mV)	I_{corr} mA cm ⁻²	Tafel Constants		R_p (Ωcm ²)	Inhibition Efficiency (%)
			$-b_c$ (mV dec ⁻¹)	$-b_a$ (mV dec ⁻¹)		
0	-490	526	136.3	133.5	17.9	-
50	-456	207	134.4	131.2	7.17	60.6
100	-469	183	132.5	128.3	6.45	65.7
150	-478	147	130.9	127.4	5.23	72.1
200	-489	121	129.3	129.5	4.30	76.9
250	-497	91.2	127.2	128.4	3.28	82.6

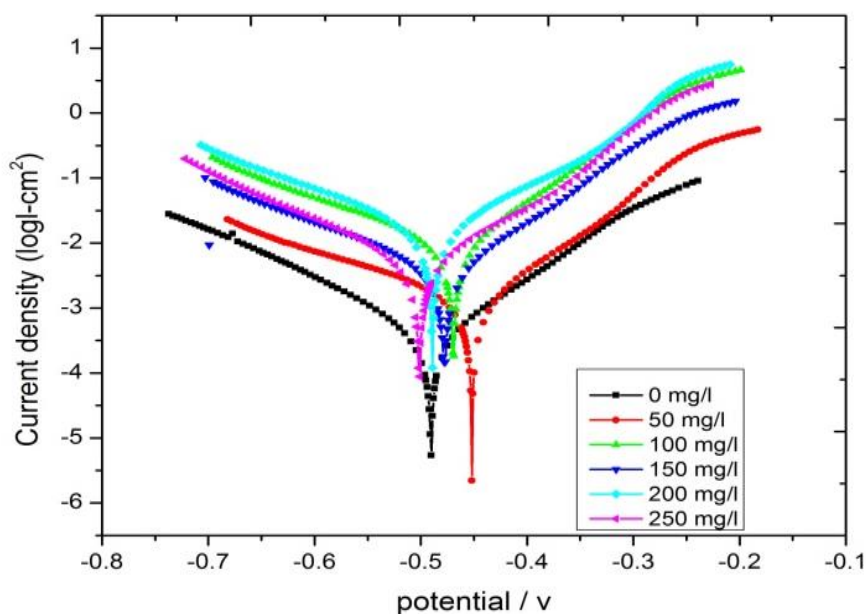


Figure .5 Tafel plot of low carbon steel immersed in 1MHCl with and without Gutle

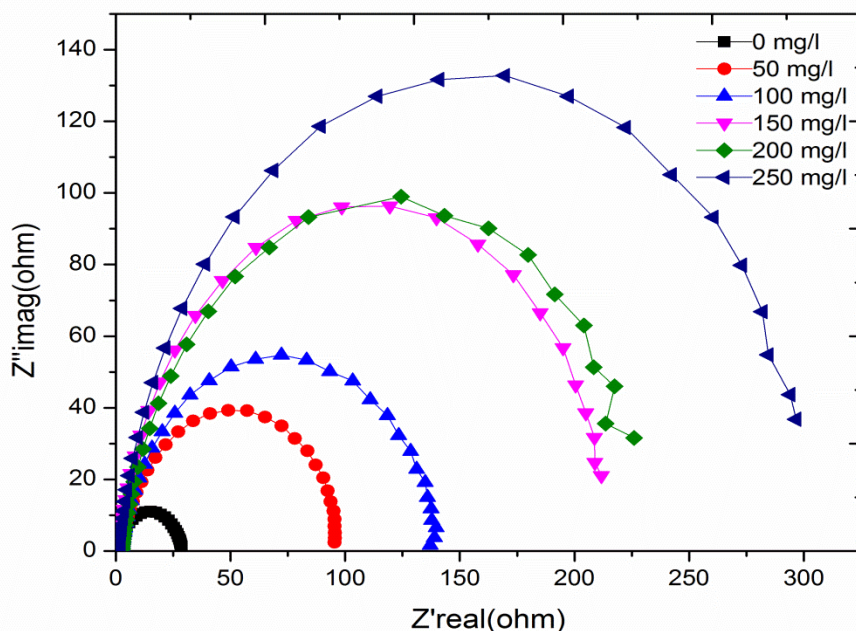


Figure .6 Nyquist plot of low carbon steel immersed in 1M HCl with different concentrations of *Gutle* at 303K

Table .3 Electrochemical impedance parameters for low carbon steel in 1M HCl in the absence and presence of *Gutle*

<i>Gutle</i> Concentration (mg)	R_{ct} (Ωcm^2)	C_{dl} ($\mu F cm^{-2}$)	Inhibition Efficiency (%)
0	28.6	403	--
50	95.6	89	70.08
100	138.9	77	79.4
150	208.9	68	86.3
200	226	53	87.3
250	296.7	43	90.3

3.4 Adsorption Considerations

One can look at adsorption isotherms to understand how the inhibitor interacts with the low-carbon steel surface. Various adsorption isotherm models, such as Langmuir, Freundlich, and Tempkin, were used to determine the extent of adsorption by using

the values of surface coverage (θ). A temp's adsorption isotherm model was used to fit the surface carbon values of low-carbon steel [18].

$$\log \theta = \log C \quad (7)$$

In the adsorption-desorption process, where $0 < n < 1$, θ represents the surface covering, C is the inhibitor



concentration, and K_{ads} is the equilibrium constant [18]. Gutle extracts at 30-60 °C are illustrated in Figure 7 by plotting $\log \theta$ against $\log C$. The adsorption parameters, including R^2 , $-\Delta G_{ads}$, K , ΔH_{ads} , and $-\Delta S_{ads}$ values,

are listed in Table 4, which was generated using the linear plots. A Temkin adsorption isotherm obeysance is indicated by an R^2 value greater than 0.9.

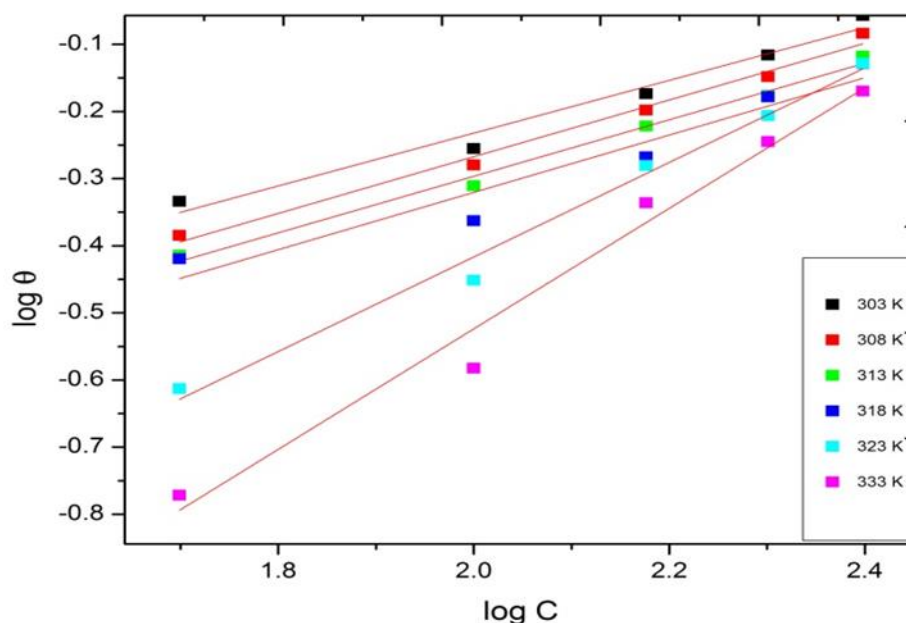


Figure .7 Temkin adsorption isotherm plot for low carbon steel in 1M HCl with Gutle extract at different temperatures

The weak connection between the adsorbed molecules and the metal surface could be why the inhibitor to the metal surface appears to diminish as the temperature increases [12]. The thermodynamic model is helpful for a better understanding of inhibitor molecule adsorption. The Van't Hoff equation [4,18] could be used to get the adsorption enthalpy

$$\ln K_{ads} = \frac{-\Delta H_{ads}^{\circ}}{RT} + constant \quad (8)$$

The plot of $\ln K$ vs. $1/T$ is shown by the straight lines in Figure 8, and the slope of these lines is $-\Delta H_{ads} / R$.

Physical adsorption is the sole mechanism for inhibitor adsorption on metal surfaces, according to the free energy values of adsorption. As free energy adsorption values as low as -20 kJ mol^{-1} indicate, physical adsorption is often associated with electrostatic interaction between charged molecules and a charged metal [26-28]. According to references [29,30], the spontaneous adsorption of the Gutle-coated low-carbon steel in HCl can be explained by a physisorption mechanism, as indicated by the negative values of ΔG_{ads} .

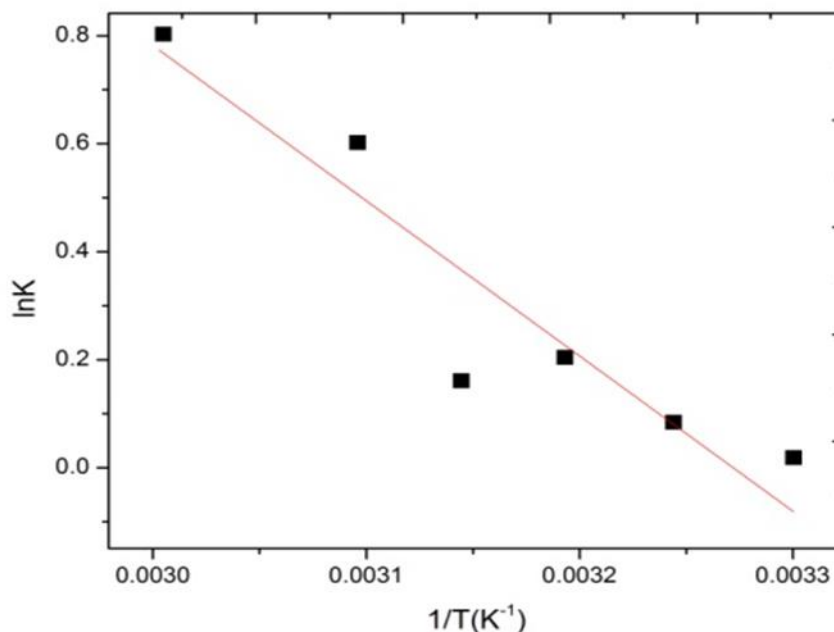


Figure .8 Plot of $\ln K$ vs. $1/T$ for the adsorption of *Gutle* at low carbon steel /HCL interface

The following equation (9) [18] relates the standard free energy of adsorption (ΔG_{ads}) to the equilibrium constant (K).

$$\Delta G = -RT \ln(55.5K) \quad (9)$$

Where R is the gas constant, T is the temperature, and 55.5 is the molar concentration of water in the solution.

The molar water concentration in the solution is 55.5, and the gas constant is R. The temperature is also mentioned. It is possible to roughly define the heat of

adsorption as the standard heat of adsorption (ΔH_{ads}) in experimental settings. The expected entropy of adsorption, denoted as ΔS_{ads} , can be calculated using (1) [18].

$$\Delta S_{ads} = \frac{\Delta H_{ads} - \Delta G_{ads}}{T} \quad (10)$$

It has been found that the values of ΔH_{ads} are positive, suggesting that the adsorption of inhibitor is an endothermic process, which means that the dissolution of

Table .4 Temppkin adsorption parameters and free energy of adsorption of *Gutle* as an inhibitor on the surface of low carbon steel

Temp(K)	$-\Delta G^{\circ}_{ads}$	K	ΔH_{ads} (kJ mol ⁻¹)	$-\Delta S_{ads}$ (J mol ⁻¹ K ⁻¹)	R ²
303	8.7	9.8	7.4×10^{-6}	33.24	0.96
308	10.0	8.9	4.1×10^{-5}	32.50	0.98
313	10.2	8.7	4.9×10^{-5}	32.69	0.98
318	10.5	8.5	6.0×10^{-5}	32.05	0.91
323	10.9	5.4	2.2×10^{-4}	28.39	0.98
333	11	4.3	3.0×10^{-4}	26.40	0.97

Low-carbon steel was slow in the presence of an inhibitor [31]. At temperatures between 303 and 333K, the values of ΔS_{ads} are negative. According to references [32,33], a decrease in disorder is observed while moving from

reactants to the activated complex since the negative values of entropies (ΔS^*) suggest that the activated complex in the rate-determining phase shows an association rather than a dissociation.



3.5. Thermodynamic Considerations

The Arrhenius Eq (11) and Transition state Eq. (12) were used to calculate the activation parameters for the corrosion process [18].

$$C_R = A_{exp} \left(\frac{-E_a}{RT} \right) \quad (11)$$

$$C_R = \frac{RT}{hN} \exp \left(\frac{\Delta S^*}{R} \right) \exp \left(\frac{-\Delta H^*}{RT} \right) \quad (12)$$

N is Avogadro's number, h is Planck's constant, T is the absolute temperature, R is the gas constant (R = 8.314 J

mol⁻¹ K⁻¹), E_a is the activation energy, and A is the frequency factor. Figure 9.0 shows the log CR vs. 1/T plot, whereas Figure 4.10 shows the log CR/T vs. 1/T plot for the Arrhenius and Transition State, respectively, with slopes of (-E_a/2.303R) and (-ΔH^{*}/2.303R), respectively. The intercepts for the Arrhenius equation and the Transition State equation will be A and [(log R/hN + (ΔS^{*}/2.303R))], respectively.

Table .5 Corrosion kinetic parameters for low carbon steel in 1M HCl in the absence and presence of different concentrations of Gutle

Cinch (mg)	-E _a (KJ mol ⁻¹)	ΔH [*] (KJ mol ⁻¹)	ΔS [*] (KJ mol ⁻¹)
0	32.7	26.72	197.59
50	36.56	58.46	197.58
100	37.42	66.45	197.58
150	38.13	68.70	197.58
200	46.25	76.04	197.58
250	55.63	118.27	197.57

Table 5 lists the computed values of E_a, ΔS^{*}, and ΔH^{*}: the activation enthalpies, activation entropies, and apparent activation energy, respectively. The formation of a stable metal-inhibitor complex causes the E_a values to rise from 32.97 to 55.6 kJ mol⁻¹, indicating that the inhibitor is more effective at inhibiting the target reaction. Enthalpies (ΔH^{*}) with positive values between 26.72 and 118.27 kJ mol⁻¹ suggest that the process is exothermic and requires more incredible energy to reach the active state or equilibrium [18]. Negative entropy values (ΔS^{*}) indicate that the association, rather than dissociation, is responsible for the activated complex in the rate-determining phase, meaning that the disorder decreases as one moves from the reactants to the activated complex [27,34].

3.6 FT-IR Studies

In Figure 11.11(a), we can see the FT-IR spectrum of the Gutle leaf extract. In Figure 11.11(b), we can see the FT-IR spectrum of the adsorbed protective layer that formed on the surface of the low-carbon steel after it was immersed in 1MHCl with 250 mg/100 ml of root. The stretching vibration of aliphatic carbonyls caused the absorption band at 1733 cm⁻¹. Analogous to an aliphatic C-NO₂ nitro molecule, the 1365 cm⁻¹ peak was observed. One possible explanation for the band at 1220 cm⁻¹ is the vibration of aliphatic C-N bonds. The stretching mode of the C-H band could explain the peak at 2929 cm⁻¹. At 1644 cm⁻¹, the peaks for stretching C=C multiple bonds were observed.

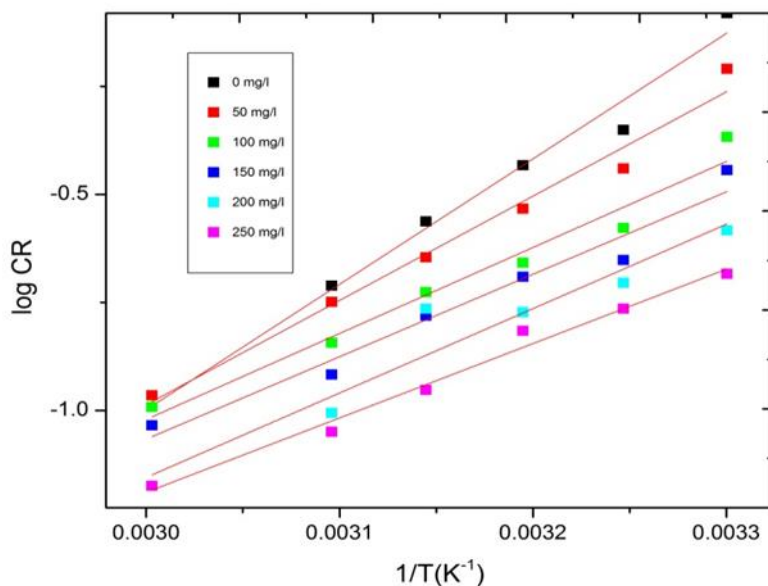


Figure .9 Arrhenius plot for low carbon steel in 1M HCl in the absence and presence of different concentrations of *Gutle*

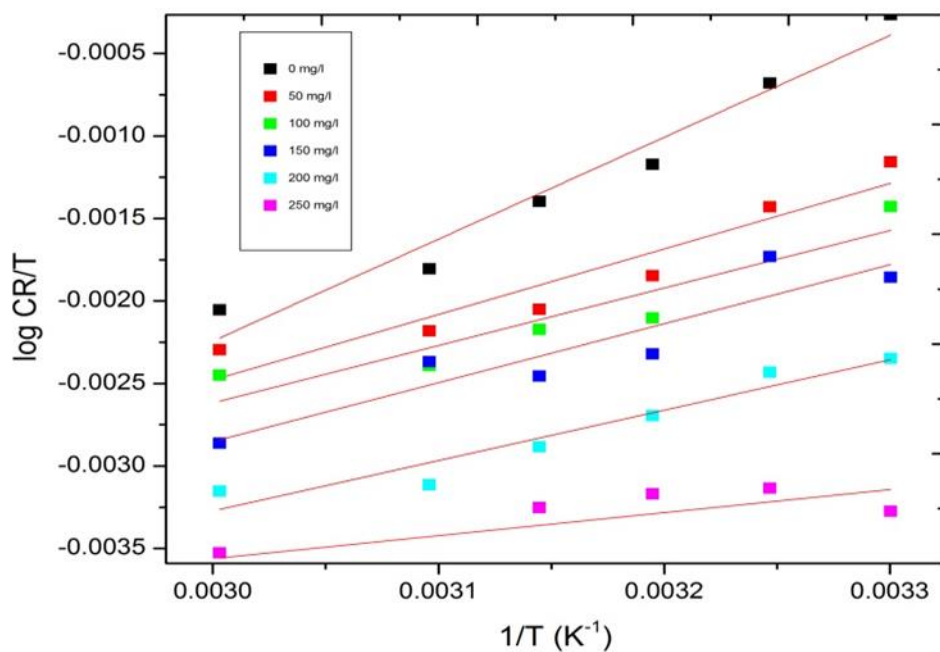


Figure .10 Transition plot for low carbon steel immersed in 1M HCl with and without *Gutle*

C-H bending mode peaks were seen at 1445 cm^{-1} . He states that at 1088 cm^{-1} and 1040 cm^{-1} , there were stretching modes for C=S. The intense stretching mode of N-H overlapped the band at 3462 cm^{-1} (related

hydroxyl). The method of bending carbon-carbon double bonds was ascribed to the band at 904 cm^{-1} . By comparing Figure 11(a) and 11(b), we can see that the metal surface had an effect of interaction or absorption,



causing specific peaks to move to a higher frequency region and others to emerge. Absorption bands at 642 cm^{-1} and 596 cm^{-1} were caused by stretching vibrations

of C=C and Fe-S, respectively. Based on the earlier observations, the metal surface appears to have a Fe^{2+} combination with an inhibitor [35].

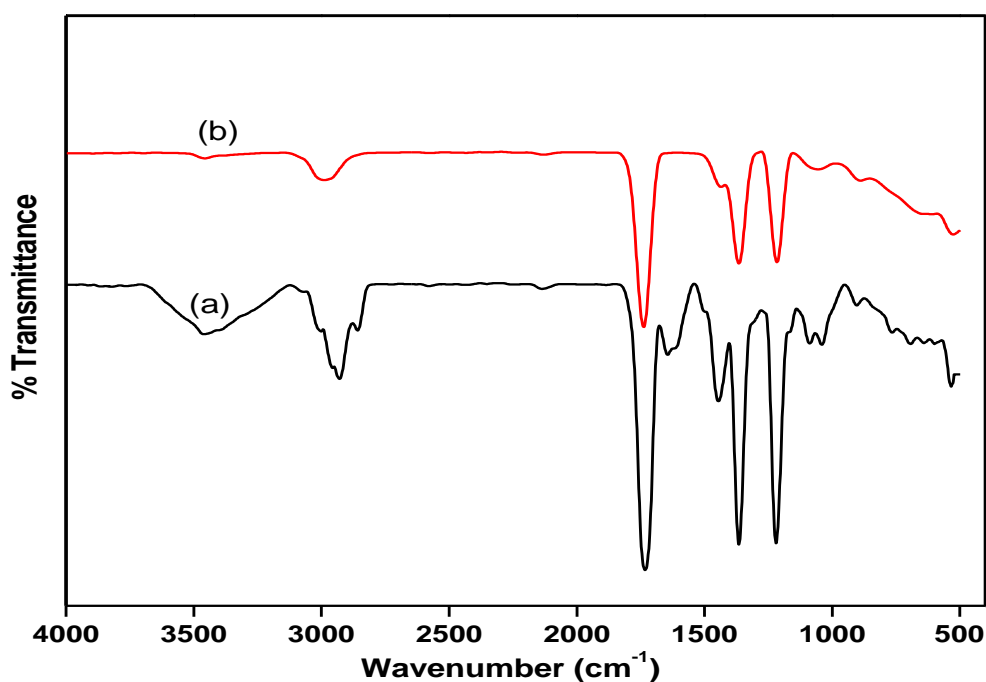


Figure .11 FTIR Spectra of (a)*Gutle* Residue (b) Adsorbed layer formed on low carbon steel after immersion in 1M HCl containing *Gutle*

3.7 EDAX Analysis

Figures 12(a) and 12(b) show the EDAX spectra of the inhibited carbon steel samples and the pure low-carbon steel samples that had rusted. The EDAX results of low-carbon steel in a 1.0M HCl acid solution, both with and without *Gutle* inhibitors, are presented in Table 4.6. Figure 12. displays spectra with oxygen and

iron peaks, which may indicate the presence of iron oxide or hydroxide following corrosion. Carbon peaks in the spectrum (Figure 12(b)) demonstrate that inhibitor molecules have been adsorbed onto the metal surface [36].

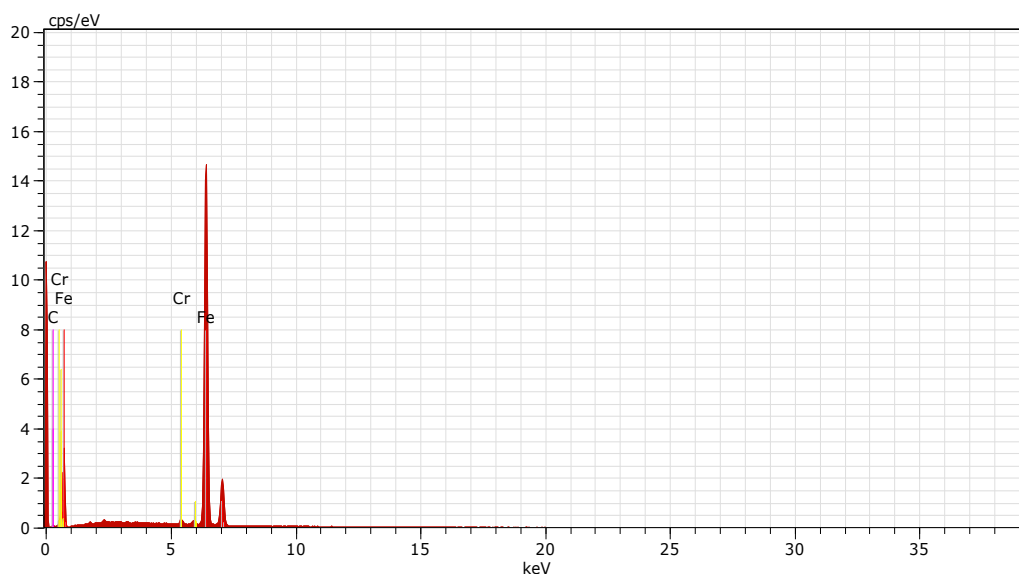


Figure .12(a) EDS Spectrum of corroded sample on low carbon steel

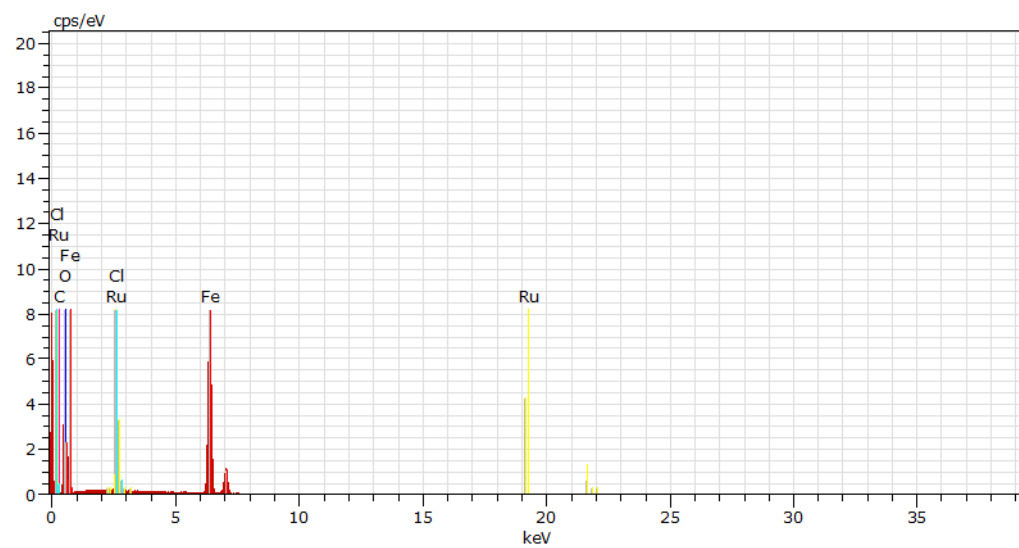


Figure .12(b) EDS spectrum of low carbon steel after treating with *Gutle* inhibitor



3.8. SEM Analysis

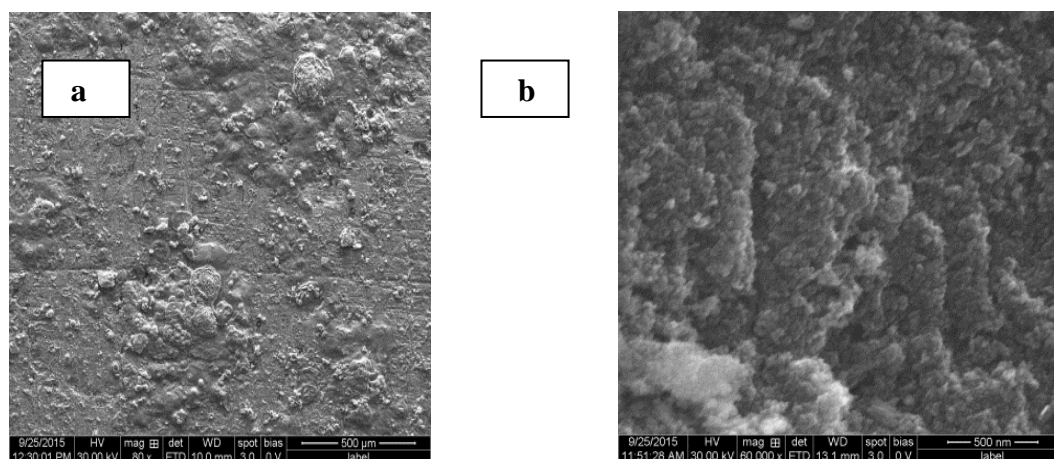


Figure .13 SEM image of low carbon steel (a) Without an inhibitor (b) 250mg/100ml of inhibitor

Table .6 Surface Composition (weight %) of low carbon steel in absence and presence of inhibitor

Medium	Composition (%)					
	Fe	C	Cr	O	Cl	Ru
Low carbon steel	92.9	4.44	0.75	-	-	-
Low carbon steel in 1.0M HCl acid in <i>Gutle</i>	48.04	6.05	-	62.08	4.30	0.55

Figure 13 (a and b) shows the results of immersing cleaned low-carbon steel in a 1M HCl solution for two hours in both the presence and absence of 250 mg/100ml of *Gutle*. Without inhibitors, metal breakdown in acid solution caused severe surface damage to low-carbon steel, as seen in Figure 13.13(a). There were deep holes, and the surface was very rough and porous. After an inhibitor is added to the solution, Figure 13.13(b) shows how the smooth and soft surfaces look. According to this finding, the presence of green *Gutle* inhibitors slowed corrosion because the inhibitor molecules attached to the metal surface formed a protective layer.



3.9. Inhibition mechanism

The primary ingredients of the gutle extract can be found as cations or neutral molecules in solutions with acidity. A variety of mechanisms exist for inhibitor adsorption on metal surfaces:

The electrostatic interaction between adsorbed chloride ions and cationic compounds,

The π -electrons of the aromatic ring and the unoccupied d orbital on the surface of iron atoms interact as donors and acceptors.

Interaction between iron surface atoms' vacant d orbitals and hetero atoms' unshared electron pairs.

Several variables can affect how an inhibitor works in acidic solutions, including the metal's type, the concentration of the extracts, the acid's anion, the existence of other species in the solution, and the amount to which the reaction forms secondary inhibitors [37]. Two possible adsorption mechanisms could be considered here:

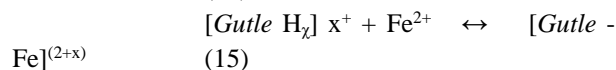
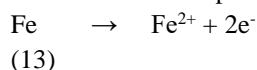
The chemisorption mechanism allows the neutral Gutle to adsorb onto metal surfaces, which involves removing water molecules from the surface and exchanging electrons between the oxygen and iron atoms. The donor-acceptor interactions between the π -electron of the aromatic ring and empty orbitals of Fe allow the Gutle molecules to adsorb on the surface of the metal itself.

Electrostatic interactions between the negatively charged metal surface and the positively charged molecules may cause the Gutle to adsorb.

Protonation causes adsorbed Gutle to form coordination bonds with metal surfaces through partial electron transfer from polar atoms (O atoms), which in turn forms metal inhibitor complexes:

A comparable process has been proposed in other works of literature [38]. Vander Waals' force may cause these complexes to be adsorbed onto the surface of low-carbon steel, where they could create a protective coating that shields the metal from corrosion. The Gutle may adsorb through electrostatic interactions between the positively charged molecules and the negatively charged metal surface.

When protonated, Gutle is adsorbed on the metal surface; a coordinate bond may be formed by partial transference of electrons from polar atoms (O atoms) to the metal surface and form metal inhibitor complexes:



Various literature has suggested a similar type of mechanism [38]. These complexes might be adsorbed on the low-carbon steel surface by Vander Waals' force to form a protective film to prevent the metal from corrosion.

4. Conclusion

1M solution of hydrochloric acid and gum extract is an effective and environmentally safe way to protect low-carbon steel from corrosion. The gut's inhibition efficacy drops with rising temperature but rises with increasing inhibitor concentration. Its maximum efficiency is 87.7 percent in 1MHCl. Adsorption by Gutle on surfaces of low-carbon steel follows the Tempkin adsorption isotherm. In 1MHCl, the gutle extract functions as a mixed-type inhibitor, and EIS spectra show that the charge transfer process regulates the corrosion response. When gutle extract is added to 1MHCl solutions, Rct values rise, and Cdl values fall. By introducing gutle extract to a 1MHCl solution, the low-carbon steel surface forms an adsorptive layer that prevents corrosion. As Cdl values fall, Rct values rise. By introducing gutle extract to a 1MHCl solution, the low-carbon steel surface forms an adsorptive layer that prevents corrosion. The adsorption is spontaneous, as shown by the negative ΔG_{ads} values. Gutle physically sticks to the surface of the low-carbon steel, as indicated by the activation energy value. Methods such as FT-IR, EDAX, and SEM were used to confirm the creation of a protective film that would shield the metal from corrosion.

12. REFERENCES

1. Ravi chandran.R., Rajendran.N., Appl. Surf. Sci., 2005,241, 449.
2. Quarishi.M.A., Ansari F.A., Jamal. D., Mater.Chem.Phys.,2002,77,687.
3. Hosseini.M., Mertens.S.F.L., Ghorbani.M., Arshadi.A.R., Mater.Chem. Phys., 2003,78,800.
4. Emregul.K.C., Hayvali.M., Corr.Sci., 2006,48,797.
5. Popova.A., Chirstov.M., Zwetanova.A., Corr. Sci.,2007,49,2131.
6. Oguzie.E.E., Mater.Chem.Phys.,2008, 99,441.



7. Valek.L., Martinez.S., Mater. Lett.,2007, 5,148.
8. Quraishi. M.A., Singh.A., Singh. V.K., Yadav. D.K., Singh. A.K., Mater.Chem.Phys., 2010,122,114.
9. Rajalakshmi.R., Subashini.S., Prithiba.A,Asian J.Chem.,2010, 22(7), 5034.
10. EkanemU.F., Umoren.S.A., Udousoro I.I., Udoh.A.P., J. Mater. Sci.,2010,45, 5558.
11. Patel.N.S., Jauhari .S., Mehta G.N.,Arab. J. Sci.,2009,34(2C) 61.
12. El-Etre. A.Y., J. Colloid. Inter. Sci.,2007,314,578.
13. Soror.T.Y., Eur. Chem. Bull.,2013,2(4),191.
14. Nnabuk O. Eddy., Femi Awe., Eno E. Ebenso., Int. J. Electrochem. Sci.,2010, 5,1996.
15. Fouda. A.S., Tawfik.H., Adv. Mater. Corros.,2012,1.
16. Sharma.M., Prasad S.B., International Journal of pharmacognosy and Phytochemical Research.,2014.,15,6(4),1010.
17. Muthukrishnan.P., Jeyaprabha.B., Prakash.P., Arab. J.chem.,2013, 08,011.
18. Muthukrishnan.P., Jeyaprabha.B., Prakash.P., Int.J.Ind.Chem.,2014, 5:5.
19. Sanja Martinez., Ivica Stern., Appl.Surf.Sci.,2002,199,83.
20. Popova.A., Okolova.E., Raicheva.S., Christov.M., Corros. Sci.,2003, 45,33.
21. Shriver. D.F., Atkins. P.W., Langford. C.H., Inorganic chemistry,2nd ed, Oxford University Press.,1994,238.
22. Singh. A.K., Quraishi. M.A., Mater. Chem. Phys.,2010, 123, 666.
23. Naqvi.I., Saleemi. A.R., Naveed.S., Int.J.Electrochem Sci.,2011,6,146.
24. Avci., Gulsen., Colloids.Surf.A.,2008, 317, 730.
25. Brighton Arul Jacob.Y., Sayee Kannan.R., Jeyasundari.J., Eur. Chem. Bull., 2013,2(5), 293.
26. Behpour.M., Ghoreishi.S.M., Khayatkashani. M., Soltani.N., Corr.Sci.,2011, 53, 2489.
27. Boukalah.M., Hammouti.B., Lagrenee. M., Bentiss.F., Corr. Sci., 2006, 48, 2831.
28. Li.X.H., Deng.S.D., Fu.H., Prog. Org. Coat.,2010,67, 420.
29. Gunavathy.N., Murugavel. S.C., E.J. Chem.,2012, 9, 487.
30. Eduok.U.M., Umoren.S.A., Udoh.A.P., Arabian. J. Chem.,2012, 5, 325.
31. Li Xianghong., Deng Shuduan., Hui Fu.,Corr .Sci.,2012,62,163.
32. Soltani.N., Behpour.M., Ghoreishi.H., Naeimi.S.M., Corr.Sci.,2010,52, 1351.
33. Gomma.M.K., Wahdan.M.H.,Mater. Chem. Phys.,1995,39, 209.
34. Fouda. A.S., Al-Sarawy. A.A., El-Katori. E.E., Desalination.,2006,201,1.
35. Li Xianghong., Deng Shuduan., Hui Fu, Li Taohong., Electrochimi Acta., 2009,54,4089.
36. Deepa Prabhu., Padmalatha Rao.,Journal of Environmental Chemical Engineering .,2013,676.
37. Leelavathi.S., Rajalakshmi.R., J.Mater.Enviro.Sci .,2013,4(5),625.
38. Xiang-Hong Li., Shu-Duan Deng, Hui Fu.,J. Appl. Electrochem., 2010,40, 1641.